View metadata, citation and similar papers at core.ac.uk

brought to you by CORE

provided by Cleveland-Marshall College of Law

Cleveland State University
EngagedScholarship@CSU

Electrical Engineering & Computer Science Faculty Publications

Electrical Engineering & Computer Science Department

1-15-2015

Dynamic Modeling, Parameter Estimation and Control of a Leg Prosthesis Test Robot

Hanz Richter
Cleveland State University, h.richter@csuohio.edu

Daniel J. Simon
Cleveland State University, d.j.simon@csuohio.edu

William A. Smith
Cleveland Clinic

Sergey Samorezov
Cleveland Clinic

Follow this and additional works at: https://engagedscholarship.csuohio.edu/enece_facpub

Part of the Electrical and Computer Engineering Commons, and the Robotics Commons

How does access to this work benefit you? Let us know!

Original Citation

H. Richter, D. Simon, W. A. Smith and S. Samorezov, "Dynamic modeling, parameter estimation and control of a leg prosthesis test robot," Appl. Math. Model., vol. 39, pp. 559-573, 2015.

Repository Citation

Richter, Hanz; Simon, Daniel J.; Smith, William A.; and Samorezov, Sergey, "Dynamic Modeling, Parameter Estimation and Control of a Leg Prosthesis Test Robot" (2015). *Electrical Engineering & Computer Science Faculty Publications*. 329.
https://engagedscholarship.csuohio.edu/enece_facpub/329

This Article is brought to you for free and open access by the Electrical Engineering & Computer Science Department at EngagedScholarship@CSU. It has been accepted for inclusion in Electrical Engineering & Computer Science Faculty Publications by an authorized administrator of EngagedScholarship@CSU. For more information, please contact library.es@csuohio.edu.

Dynamic modeling, parameter estimation and control of a leg prosthesis test robot

Hanz Richter, Dan Simon, William A. Smith, Sergey Samorezov

1. Introduction

Concepts for advanced prosthetic devices have been developed at a very fast pace in recent years. In particular, the literature continues to report significant progress in passive, semiactive and fully-active leg prostheses [1–7]. These advances are evident at all technology readiness levels, from conceptual design and mathematical models to demonstrated prototypes. Concomitant to these developments arises the need for systematic prototype testing programs. During the product development phase, testing under normal and hazard conditions involving patients is problematic. Legal clearance burdens, required safety harnesses and a lack of repeatability across test subjects place significant restrictions on the scope of the tests that may be conducted and the quality of the data being gathered.

Robotic testing can eliminate or reduce many of these obstacles and bring additional benefits. For instance, robots may be commanded to simulate conditions which are deemed unsafe for patients, such as near-fall situations. A robot may be operated continuously for long periods of time, as necessary for certain real-time optimization of prosthetic control algorithms [8] or to evaluate the mechanical endurance of a prototype. Also, robots may be fitted with sensors to measure quantities of interest which are difficult to measure directly in a human subject, such as hip torque and angle. Finally, performance comparisons among various candidate designs can be conducted in a meaningful way only if controlled test conditions are assured, with sufficiently large trial data sets.

Although some use of commercial manufacturing robots in prosthesis testing has been reported by the Fraunhofer Institute [9] and the Cleveland Clinic [10], the use or development of a machine aimed at reproducing prosthetic gait has not been reported, to the best of the authors' knowledge. In this paper, robotic testing of transfemoral prosthesis is proposed, and the development, modeling and control of a two-degree-of-freedom robot to emulate hip motions is described. It is expected that robotic testing of prostheses will play a major role in evaluating the dynamic characteristics of prototypes because the input displacements, velocities, accelerations, torques and forces can be measured with much more accuracy and repeatability than during human gait trials.

The robot described in this paper is designed to test transfemoral prostheses [11]. A simple passive knee with a blade foot is used to illustrate the approach to modeling and control and to conduct proof-of-concept tests with the newly designed robot. However, any prosthesis, including powered knee-ankle devices can be attached to the machine and the model can be modified to reflect the dynamics of the prosthesis in use. Irrespective of the kind of prosthesis attached, the robot has full authority over hip vertical displacement and thigh angle. In this paper we consider pure motion tracking for these two degrees of freedom, but the actuation, sensing and control hardware are ready for objectives other than trajectory control, for instance force control, hybrid force/trajectory control and impedance control.

The sample test modality used in the experimental section of this paper is to track hip displacement and thigh angle data gathered from able-bodied subjects walking normally. Since a passive knee was used, knee angle and ground force profile are observed variables that can be compared against able-bodied data matching normal walk data. This comparison provides an indication of the prosthesis' gait fidelity. Other tests and studies can be conducted by suitably changing the control objective and algorithm, the sensed variables used for feedback and/or the tracking references. For instance, combined hip motion and ground reaction control has been achieved with this machine [12]. In this modality, a passive prosthesis is also used and a set of baseline hip displacement and thigh angle references are used. Active biasing of the baseline references is performed using online evolutionary optimization so that ground reaction force tracks a ground reaction profile corresponding to the same able-bodied walking data. This study provides insight about the compensation that a patient would need to apply to reproduce normal gait while wearing that specific prosthesis. These kinds of studies have so far relied on patient trials or biomechanical models [13–17].

The overall design of the robot responds to high-level requirements such as the number of degrees of freedom, the shape of the motions to be generated and load capacity requirements, which leave few options for the mechanical configuration. Upon fixing the kinematic concept, electromechanical actuation was favored over hydraulics due to the higher achievable positioning accuracy and generally faster control bandwidth of the former. Besides, a hydraulic system requires several ancillary components such as pumps, a tank, valves and filters, resulting in a bulkier and overall less efficient solution for this particular application. Installation of a hydraulic system in a clinical research facility may not be feasible due to noise and cleanliness concerns. This paper focuses on the modeling, parametric estimation and baseline feedback control of the robot. The remainder of the paper is organized as follows: Section 2 describes machine functionality and components; Section 3 first derives separate models for the machine and for the prosthesis, and then integrates them into one, following a robotic manipulator dynamics framework; Section 4 describes various parameter estimation procedures used to populate the dynamic model; Section 5 presents preliminary independent-joint controller that can be used to accurately track motion profiles; Section 6 reports our success in achieving the desired motion profiles and Section 7 offers conclusions and some recommendations for future improvements to the design and possible test modalities.

2. Machine design

The robot must produce motions that mimic those of a human hip during walking and running. This design is limited to two degrees of freedom, namely hip vertical displacement and hip swing, which are the minimum required to reproduce two-dimensional gait patterns. Normal hip displacement and swing are periodic oscillations with amplitudes and waveforms that depend primarily on the height of the patient and the walking or running speed. Normal gait profiles used as a guideline for design are a subset of the data collected by van den Bogert [18], which includes walking and running in healthy subjects. The machine is designed for hip displacement amplitudes of up to 50 mm, with a maximum velocity of 1 m/s. Vertical force capacity is specified at 1200 N, which exceeds the ground force generated by a 78 kg normal subject during fast walk/slow running. The vertical motion stage is comprised of a DC motor, a ballscrew and a linear slide. Overall vertical motion range is 12 inches, of which up to 100 mm are used to accommodate the expected vertical hip motion profiles. The remaining space is used to shift the center of oscillation, as it may be required to test prostheses of various lengths. The center of oscillation may also be changed during real time operation to initiate and regulate contact between the foot and the walking surface. Since the machine has a fixed vertical axis, a treadmill is used as a walking surface.

The rotary motion stage, including motor, is carried by the vertical slide. Prostheses are attached to the rotary plate by means of an adjustable threaded rod, which is secured to a bracket on the plate with two 2.75-inch nuts. The threaded rod, in combination with the adjustable center of oscillation of the vertical stage, offer great flexibility for standoff adjustments. Although thigh angular excursion in the normal gait data does not exceed 50 degrees, the rotary actuator has an unlimited angular range. Following biomechanical data from [18], the design values for thigh angular velocity and torque are is 150 degrees per second and 75 Nm.

A schematic diagram of the robot and its components is shown in Fig. 1, and the finished machine is shown in the photograph of Fig. 2.

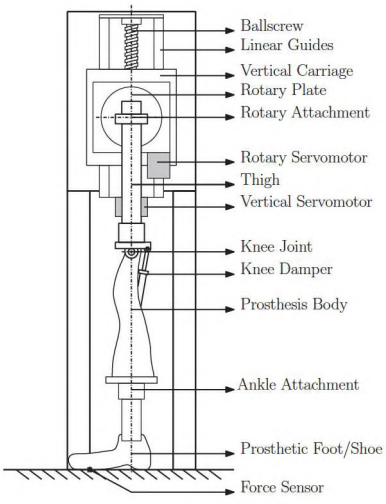

Fig. 1. Machine Schematic.

2.1. Support structure

The linear slide is attached to a rigid frame built with A500 rectangular steel tubing. Frame elements are welded together, and bolted joints are used for the mounting plates. The frame, the welds and the bolted joints were verified for static loading and fatigue using the SolidWorks software. A treadmill is secured to the frame by bolts, and anchor bolts are used to secure the entire assembly to the lab floor. Overall machine dimensions are $48'' \times 61'' \times 26''$.

2.2. Servo systems

The vertical servo system is composed of a ballscrew-driven vertical slide (manufactured by RAF Automation, Solon, Ohio), directly coupled to a brushless DC motor (Mitsubishi HF-KP73). The motor is powered by a torque-mode servo amplifier (Mitsubishi MR-J3-70A). An analog input voltage applied to the servo amplifier results in a proportional torque on the motor shaft and ballscrew. Vertical position (hip displacement) is measured with a 1000 line/rev incremental encoder rotating synchronously with the motor. An absolute position reference is established with a limit switch mounted on the vertical guides. The ballscrew has a diameter of 1 inch, a lead of 0.5 inches per revolution and the total useful travel of the slide is 12 inches.

The rotary servo system is composed of a brushless DC motor (ElectroCraft RapidPower RP34) coupled to a rotary plate through an inchworm-gear reducer with ratio 80:1 (RM-8-SM-34, manufactured by Newmark Systems, Rancho Santa

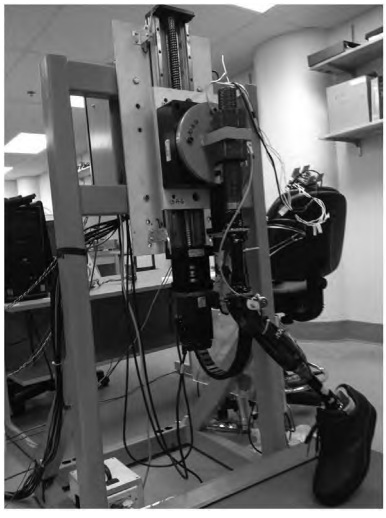

Fig. 2. Overall robot installation. A Mauch MicroLite S knee, a plastic prosthetic foot and an ortopedic shoe are installed.

Margarita, California). Angular position (thigh angle) is measured with an incremental encoder rotating synchronously with the motor. An absolute position reference is established with a limit switch mounted on the rotary plate. Real-time instrumentation and control is handled by a dSPACE DS-1102 system and associated software. The developer may easily convert Matlab/Simulink code into user-friendly real-time operating interfaces.

3. Robotic modeling

The overall machine-and-prosthesis system is best modeled in the standard framework of robotics. Indeed, the system fits the category of a 3-link rigid robot with a prismatic-revolute-revolute (PRR) configuration. When a conventional leg prosthesis is attached, the system is underactuated, since the torque of the knee joint may not be externally controlled. When advanced prototypes featuring actively-controlled knee damping are attached, the system can be regarded as fully-actuated. A general dynamic model [19] for the robot is given in joint coordinates as

$$D(q)\ddot{q} + C(q,\dot{q})\dot{q} + B(q,\dot{q}) + J_e^T F_e + g(q) = F_a, \tag{1}$$

where $q^T = [q_1 \;\; q_2 \;\; q_3]$ is the vector of joint displacements (in our case q_1 is the vertical displacement, q_2 is the thigh angle and q_3 is the knee angle), $D(q)$ is the inertia matrix, $C(q,\dot{q})$ is a matrix accounting for centripetal and Coriolis effects, $B(q,\dot{q})$ is a nonlinear damping matrix (in our case due to the knee damper), J_e is the kinematic Jacobian relative to the point of application of external forces F_e, $g(q)$ is the gravity vector and F_a is a vector of net actuator inputs, including their inertial and frictional effects. The explicit form of F_a is developed below. Matrices $D(q)$, $C(q,\dot{q})$ and $g(q)$ are readily obtained using the standard Euler–Lagrange approach. Their entries are listed in the appendix. Matrix $B(q,\dot{q})$ is specific to the leg prosthesis and discussed in Section 3.3. The external force Jacobian and the external force vector are discussed next.

3.1. Forward kinematics

A set of reference frames is defined to establish a basis for dynamic model derivations and to keep track of leg geometry during analysis, simulation and real-time operation. The frame assignments shown in Fig. 3 follow the standard Denavit–Hartenberg convention [20]. The frame-to-frame transformations matrices are expressed in terms of standard primitives [19] as:

$$A_1^0 = (\mathrm{Trans}_{z,q_1})(\mathrm{Rot}_{x,90}), \tag{2}$$

$$A_2^1 = (\mathrm{Rot}_{z,q_2})(\mathrm{Trans}_{z,d_0})(\mathrm{Trans}_{x,l_2}), \tag{3}$$

$$A_3^2 = (\mathrm{Rot}_{z,q_3})(\mathrm{Trans}_{x,c_3}), \tag{4}$$

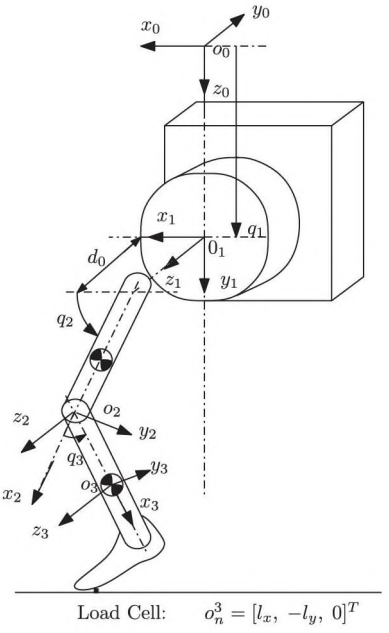

Fig. 3. Denavit–Hartenberg coordinate frame assignments.

where l_2 is the length of link 2 (thigh), d_0 is the offset of link 2 and c_3 is the distance between the knee joint and the center of mass of link 3. The world-frame coordinates of points of interest can be readily computed using the above transformation matrices, assuming q is known. The world position of the foot-mounted load cell is particularly useful when designing force feedback controls. In frame 3 coordinates, the load cell is located at $[l_{cx} \ -l_{cy} \ 0]^T$. Using the composite transformation from frame 3 to the world frame, the vertical coordinate of the load cell is found as

$$Z_{LC} = q_1 - l_{cy}\cos(q_2+q_3) + (c_3+l_{cx})\sin(q_2+q_3) + l_2\sin(q_2). \tag{5}$$

In the modeling and simulation stage, this coordinate may be compared to the treadmill's standoff height to determine belt deflection and estimate the vertical component of ground reaction force, F_{GV}. In a simplified point-foot model, the belt is regarded as a stiffness, returning a force proportional to deflection. Also, side forces (in the world Y-direction) are ignored. The friction force due to non-slip contact between belt and foot in the world X-direction is denoted by F_{GH}. This input affects knee angle, but its effect on thigh angle is negligible due to non back-driveability of the rotary actuator. Likewise, F_{GH} has no effect on the vertical actuator. As explained in Section 3.5, a kinematic constraint associated to the foot-treadmill contact eliminates the need to compute F_{GH} during simulation. In this paper, no external torques are considered at the location of the load cell, but they can certainly be incorporated if J_e is appended with the appropriate angular velocity Jacobian. Thus, we consider a force vector of the form $F_e^T = [0\ 0\ -F_{GV}]$. The velocity Jacobian at the load cell location is listed in the appendix.

3.2. Servo system models

The servo systems are modeled as current-driven DC machines with inertias attached to their shafts by a mechanical transmission. For the linear actuator, we consider Coulomb friction on the carriage guides and neglect viscous damping effects. For the rotary actuator, we consider viscous damping in the rotating gear.

3.2.1. Vertical stage

The torque balance equation on the ballscrew is $T_{m_1} - T_r = J_b\ddot{\theta}$, where T_{m_1} is the torque applied by the motor, T_r is the torque due to the interaction between ballscrew and carriage nut, J_b is the moment of inertia of the ballscrew and θ is the rotation angle. A transmission screw of pitch radius r and lead l (in units of length per revolution) exhibits a linear torque-force relationship [21] of the form:

$$F = \frac{1}{\gamma}T_r, \tag{6}$$

where $\gamma = \frac{l}{2\pi r\eta}$, F is the thrust force and η is an efficiency figure, typically between 0.8 and 0.9 for ballscrews. Using the ballscrew lead, we have $\theta = q_1/l$. Also, we define and calibrate the servo amplifier constant through the relationship $T_{m_1} = \gamma k_1 u_1$, where u_1 is the analog control voltage and k_1 is a constant. The force exerted by the ballscrew on the carriage becomes:

$$F = k_1 u_1 - m_0\ddot{q}_1, \tag{7}$$

where $m_0 = J_b/(\gamma l)$ represents an inertial parameter which is not subject to gravity.

3.2.2. Rotary stage

The rotary servo system can be modeled by the transfer function

$$G_2(s) = \frac{W_2(s)}{U_2(s)} = \frac{k_2}{(J_o + i^2 J_m)s + b_r}, \tag{8}$$

where $W_2(s)$ and $U_2(s)$ are the Laplace transforms of the thigh angular speed and rotary actuator control voltage, respectively, k_2 is the servo amplifier gain (in N-m per volt), J_o is the rotary inertia associated with the actuator gear, mounting plate and accessories, $i = 80$ is the gear ratio, J_m is the moment of inertia of the worm gear and motor armature, and b_r is a viscous damping coefficient associated with the rotation of the gear (friction on the motor side is small in comparison, and can be safely neglected).

3.3. Prosthesis model

A passive prosthetic leg was attached to the machine to test the modeling approach and operate the machine in real-time with a preliminary control system. The Mauch MicroLite S [5] leg consists of two rigid links connected by a hinge. A damper is connected between the links, as shown in Fig. 1, to stabilize the knee during the stance phase and limit knee angle during the swing phase. Typically, higher damping is required during the stance phase than in the swing phase. For this reason, the damper features two adjustment dials that can be used to set separate damping coefficients for knee flexion (q_3 increasing) and knee extension (q_3 decreasing).

The prosthesis, therefore, is regarded as links 2 and 3 of the overall robot. Joint 3 is subject to an internal torque due to damper action. This nonlinear damping torque can be calculated as $\partial\mathcal{R}/\partial\dot{x}_d$, where $\mathcal{R}$ is the Rayleigh dissipation function:

$$\mathcal{R} = \frac{1}{2} b_k \dot{x}_d^2, \tag{9}$$

where b_k is the direction-dependent damping coefficient and $\dot{x}_d$ is the expansion rate of the damper. The expansion rate is readily found by considering the geometry of the damper attachment and using differentiation of the cosine law. The nonlinear damping term of Eq. (1) is thus found to be:

$$B^T(q,\dot{q}) = \left[0\ 0\ -\frac{b_k o_d^2 r_d^2 \cos^2(q_3)\dot{q}_3}{l_d^2}\right], \tag{10}$$

where o_d, r_d and l_d are the damper offset, swing radius and instantaneous damper length, as shown in Fig. 4. In the absence of manufacturer's data, a custom experimental procedure described in Section 4 was used to estimate b_k.

3.4. Overall swing-mode model

With a passive knee, the actuator input term F_a in Eq. (1) has the form $F_a^T = [(F - f_f)\ T\ 0]$, where f_f is the Coulomb friction force on the linear guides and T is the net torque of the rotary stage. The Coulomb friction force is assumed to have the ideal form $f_f = f\,\mathrm{sign}(\dot{q}_1)$, where f is the magnitude of the force. From Eq. (7), the first component of F_a in Eq. (1) becomes

$$F_a(1) = F - f_f = k_1 u_1 - f\,\mathrm{sign}(\dot{q}_1) - m_o \ddot{q}_1. \tag{11}$$

To integrate the rotary actuator model into the robotic model we note that a net torque balance on the motor and worm gear axis yields $T_{m_2} - T_L = J_m \ddot{q}_{m_2}$, where $T_{m_2} = k_2 u_2 / i$ is the motor torque reflected to the output, and T_L is the load torque on the same axis. On the link axis, this torque is multiplied by i to obtain T, the net torque acting on link 2:

$$T = iT_L = iT_{m_2} - i^2 J_m \ddot{q}_2 = k_2 u_2 - i^2 J_m \ddot{q}_2. \tag{12}$$

When F_a is substituted into Eq. (1), a re-arrangement of terms yields the final dynamic model:

$$M(q)\ddot{q} + C(q,\dot{q})\dot{q} + B(q,\dot{q}) + F_f(\dot{q}) + J_e^T F_e + g(q) = Ku, \tag{13}$$

where $F_f^T(\dot{q}) = [f\,\mathrm{sign}(\dot{q}_1)\ 0\ 0]$, $K = \mathrm{diag}\{k_1, k_2, 0\}$ is the matrix of servo amplifier constants, $u = [u_1\ u_2\ 0]$ is the vector of control voltages and the inertial contributions from the robotic links and the servo system elements are combined into the mass matrix as follows:

$$M(q) = D(q) + \mathrm{diag}\{m_0, i^2 J_m, 0\}, \tag{14}$$

where m_0 is the inertial (not subject to gravity) contribution of the vertical motor armature and ballscrew, discussed in Section 3.2, i is the gear ratio of the rotary actuator, J_m is the armature inertia of the rotary actuator motor and $D(q)$ is the inertia matrix associated with the three robotic links. Eq. (13) is expressed in state-space form as:

$$\dot{z} = w, \tag{15}$$

$$\dot{w} = M^{-1}(Ku - B - Cz_2 - F_f - J_e^T F_e - g(q)), \tag{16}$$

where z is the vector of joint coordinates and w is the vector of joint velocities. The vertical component of ground force is calculated as $F_{GV} = k_b|s_z - Z_{LC}|$ when $Z_{LC} > s_z$ and otherwise $F_{GV} = 0$, where the constant s_z is the treadmill standoff (vertical distance between the origin of coordinates and the belt) and k_b is the belt stiffness.

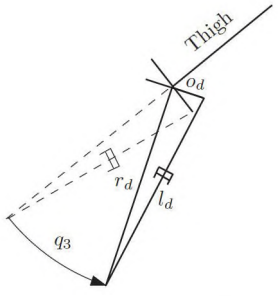

Fig. 4. Damper extension geometry.

3.5. Hybrid swing-stance model

Although the model derived in the previous sections accounts for the external ground reaction force, it does not incorporate any constraint due to the interaction of the foot and the moving surface of the treadmill. However, tests are conducted with a ground force which is sufficiently large to prevent slippage between the foot and the treadmill belt. Therefore, the horizontal component of foot velocity is constrained to match that of the treadmill belt during the stance phase. The foot is still allowed to deflect the belt in the vertical direction, giving rise to the vertical component of the contact force. As done earlier, it is assumed that this component is a purely elastic effect. The horizontal velocity of the load cell point on the foot can be readily obtained from the Jacobian listed in the appendix as:

$$\dot{x}_{lc} = -(\dot{q}_3 + \dot{q}_2)\left[(c_3 + l_{cx})\sin(q_2 + q_3) - l_{cy}\cos(q_2 + q_3)\right] - l_2\dot{q}_2\sin(q_2). \tag{17}$$

To enforce the constraint, $\dot{x}_{lc}$ is equated to $-V_H$, the treadmill speed. Then Eq. (17) is solved for $\dot{q}_3$, yielding the desired algebraic equation:

$$\dot{q}_3 = h_{VH}(q_2, q_3, \dot{q}_2). \tag{18}$$

Eq. (18) is integrated during simulation to obtain q_3. That is, knee velocity is not calculated dynamically but algebraically during stance, from the kinematic constraint. Knee velocity is the integrated to give knee angle as before. This implies that only 5 states are required during stance ($q_1, q_2, \dot{q}_1, \dot{q}_2$ and q_3), while 6 are needed in the swing phase. A discrete variable i_g which governs the transitions between swing and stance completes the description of the swing-stance model as a *hybrid dynamical system*. We define the *gait phase index* i_g as zero whenever the vertical reaction force is positive (stance phase), and as 1 if the force is zero (swing phase). Define the components of the state vectors as $z = [z_1\ z_2\ z_3]^T = [q_1\ q_2\ q_3]^T$ and $w = [\dot{q}_1\ \dot{q}_2\ \dot{q}_3]^T$ and let

$$M^{-1}(Ku - B - Cz_2 - F_f - J_e^T F_e - g(q)) = [p_1(z,w)\ p_2(z,w)\ p_3(z,w)]^T. \tag{19}$$

In swing mode, z is integrated from w, which in turn is integrated from the accelerations $p_i(z,w)$ for $i = 1, 2, 3$. In the stance mode, z_1 and z_2 are integrated from w_1 and w_2, but z_3 is integrated from the kinematic constraint of Eq. (18), and w_3 becomes unnecessary. The other two angular velocities are integrated from their corresponding accelerations, as in the swing phase. Fig. 5 is a graphical representation of the hybrid model.

3.6. Model extensions

A *point-foot* model has been used in the paper, since this is deemed sufficient to meet the objectives of hip and thigh motion tracking using a robust controller. The experimental results of Section 6, confirm this. If prosthetic ankles are used, (passive or powered) it is necessary to extend the model to account for the kinematics and dynamics of ground interaction. A wide variety of models are available that can be used, for instance [22–24].

4. Parameter estimation

4.1. Ballscrew torque/thrust constant and friction force

A custom fixture was built to measure parameter γ in Eq. (6). The ballscrew was loaded statically by pressing the carriage against a load cell, recording thrust and torque (with a separate torque cell). The value of γ was measured by linear regression to be 0.0024. This corresponds to an efficiency of 0.84 as calculated from Eq. (6), which falls in the expected range. With zero load and the slide in a horizontal position, a breaking torque must be applied to the ballscrew in order to initiate carriage motion. We regard this torque to correspond to static friction torque on the linear guides only. The breaking torque

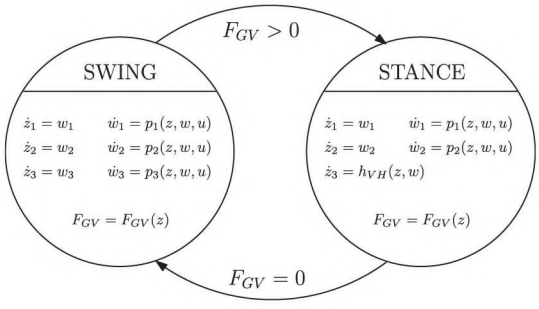

Fig. 5. Swing/stance model as a hybrid dynamic system.

was measured repeatedly using the torque cell, yielding an average value of 0.2 Nm. From Eq. (6), the static friction force on the linear guides can be estimated as $f = 83.33$ N. Note that f is likely to decrease once the carriage starts moving. Since the main purpose of the model is to facilitate controller designs, we regard the magnitude of the friction force to be constant under static or dynamic conditions, a conservative assumption.

4.2. Vertical actuator

The mass of the vertically-moving elements is not reported by the manufacturer and cannot be measured directly without disassembly. However, the vertical slide is back-driveable, i.e., the carriage will move and turn the ballscrew when a force parallel to its axis is applied. This feature can be used to estimate the vertically-moving mass by allowing the carriage to move downward under the action of gravity while recording its velocity. The motor is powered off, contributing only the inertia of its rotor. The governing equation for downward motion in the free-fall test is:

$$\left(m + \frac{J}{\gamma l}\right)\dot{v} = mg - f, \tag{20}$$

where v is the velocity of the carriage (positive downward), f is a Coulomb friction force (dominant over viscous forces in this system) and m is the vertically-moving mass (subject to gravity) and J is the sum of moments of inertia of the motor and ballscrew. The downward acceleration $\dot{v}$ is obtained by numerical differentiation of the captured velocity data. The ballscrew inertia is estimated with a standard formula [25] as $J_b = 9.65 \times 10^{-5}$ kg-m^2 and manufacturer data is used for the motor inertia, yielding $J = 2.59 \times 10^{-4}$ kg-m^2. Since f has been already calculated, the linearly-moving mas can be solved from Eq. (20) as $m = 21.3$ kg.

Once the mass and friction parameters are known, k_1 may be estimated by loading the carriage statically against a load cell in a horizontal position, recording the applied voltage and the resulting force. The voltage-force curve is roughly linear, with a linear fit slope of $k_1 = 482$ N/V. This value is adopted for the nominal model used in controller design. Subsequent tests show that the controller is robust enough to accommodate the uncertainty in this amplifier gain.

4.3. Rotary actuator

The transfer function of Eq. (8) was measured by applying a swept-sinewave signal $u_2(t)$ and recording the resulting output $\tilde{q}_2(t)$, followed by a standard system identification technique. The measured transfer function was

$$G_2(s) = \frac{1}{0.1s + 0.65}. \tag{21}$$

Note that the above data determines only the ratios $(J_o + i^2 J_m)/k_2$ and b_r/k_2. However, k_2 was measured directly by attaching a bar to the actuator and loading it statically against a load cell, measuring the applied voltage and corresponding torque. The servo amplifier was found to have an approximately linear torque-voltage curve, with an average sensitivity of $k_2 = 15$ N-m/V. This value is then used to find b_r and J_o, since J_m is known from the motor manufacturer data.

4.4. Prosthesis parameters

Link lengths l_2 and l_3 and masses m_2 and m_3 were measured directly, while the locations of the centers of mass were determined by balancing the disassembled links on a knife edge. Since the moment of inertia and mass of the rotary actuator's gear, mounting plate and mounting rod are much larger than those of the prosthetic thigh, the moment of inertia of link 2 at the center of mass was assumed to coincide with the moment of inertia at the axis of rotation: $I_{2z} = J_o + J_r$, were J_r is the moment of inertia of the connecting rod and nuts, measured in SolidWorks as 0.105 kg-m^2. To determine the moment of inertia I_{3z}, the link was suspended and allowed to oscillate in a compound pendulum fashion. The period of oscillation and the distance between the suspension point and the center of mass were used to calculate the moments of inertia using the well-known period formula. The values of damper constant were determined for each dial setting using a custom fixture. The damper was fitted with a load cell to measure axial force, and a laser sensor was used to capture displacement. Damper extension and force were recorded as the damper was manually extended and compressed. Numerical differentiation was used to obtain velocity histories, which were linked to force by linear regressions. This was done for positive and negative velocities separately, yielding two sets of values for b_k. Key model parameters and their values have been listed in Table 1.

4.5. Model validation

The model is evaluated for its ability to capture the essential dynamic interactions between the robotic links, as this is most useful for the purposes of control design. Model parameters are subject to significant uncertainty, and open-loop prediction quality is strongly dependent on the choice of parameters. The model, with nominal parameters, was used to design and simulate a closed-loop controller, as described in Section 5. The controller was then deployed in real time and plant outputs were compared with the corresponding simulation outputs. As it can be seen in Figs. 6–8, model predictions are more accurate for actively-controlled outputs than for knee angle.

Table 1
Key model parameters.

Parameter	Value	Units	Parameter	Value	Units
$\frac{J_h}{\gamma l}$	53.49	kg	l_2	0.425	m
m_1	21.29	kg	l_3	0.527	m
m_2	8.57	kg	c_2	−0.339	m
m_3	2.33	kg	c_3	0.320	m
I_{2z}	0.435	kg-m^2	r_d	0.190	m
I_{3z}	0.062	kg-m^2	o_d	0.029	m
J_m	1.82×10^{-4}	kg-m^2	b_r	9.75	N-m-s
f	83.33	N	b_k	427.7–2776.6	N-s/m

5. Independent-joint control system

The overall prosthetic testing concept is demonstrated by using a basic control system to track realistic motion profiles. Since the rotary actuator is non back-driveable, the inertial coupling due to vertical motion and leg swinging can be ignored. This implies that the rotary actuator can be controlled using a local, single-input single-output (SISO) servo loop. Similarly, leg swinging is deemed to produce small inertial forces on the vertical servo system, therefore a sufficiently robust SISO controller may be used to track vertical hip displacement profiles.

Sliding Mode Control (SMC) was chosen as a development controller due to its good robustness properties and straightforward implementation [26–28]. Neglecting inertial coupling, each joint is assumed to follow a single-axis linear electromechanical model of the form

$$J\ddot{\theta} + b\dot{\theta} = ku + \tau_d, \tag{22}$$

where $\theta(t)$ is the controlled position variable, $u(t)$ is the control voltage (assumed proportional to motor torque), k is a constant reflecting a combination of servo amplifier gain, motor torque constant and rotary/linear motion conversion, J is the inertia of the load and motor and b is a viscous damping coefficient. Variable τ_d represents an uncertain torque input consisting of actual external torque disturbances, unmodeled dynamics, parametric uncertainties and unmodeled static

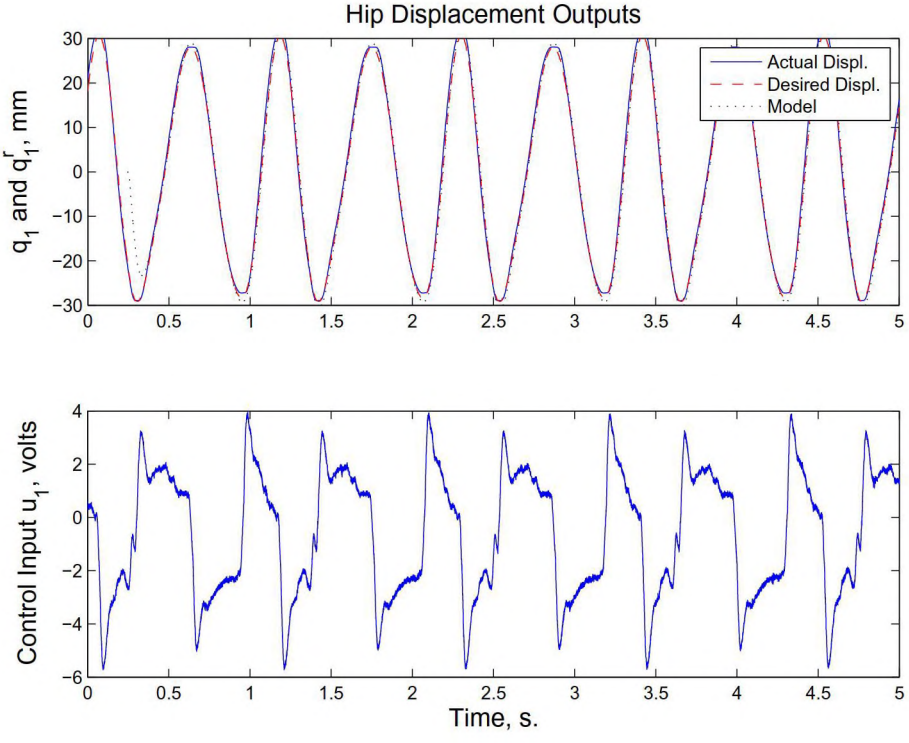

Fig. 6. Comparison between model and experimental outputs: hip displacement.

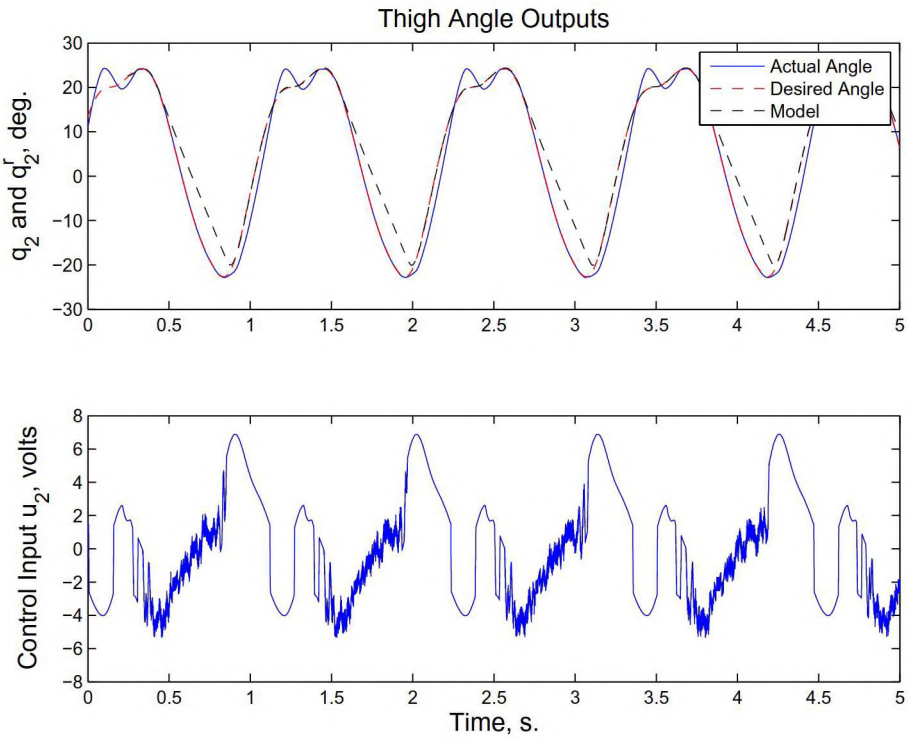

Fig. 7. Comparison between model and experimental outputs: thigh angle.

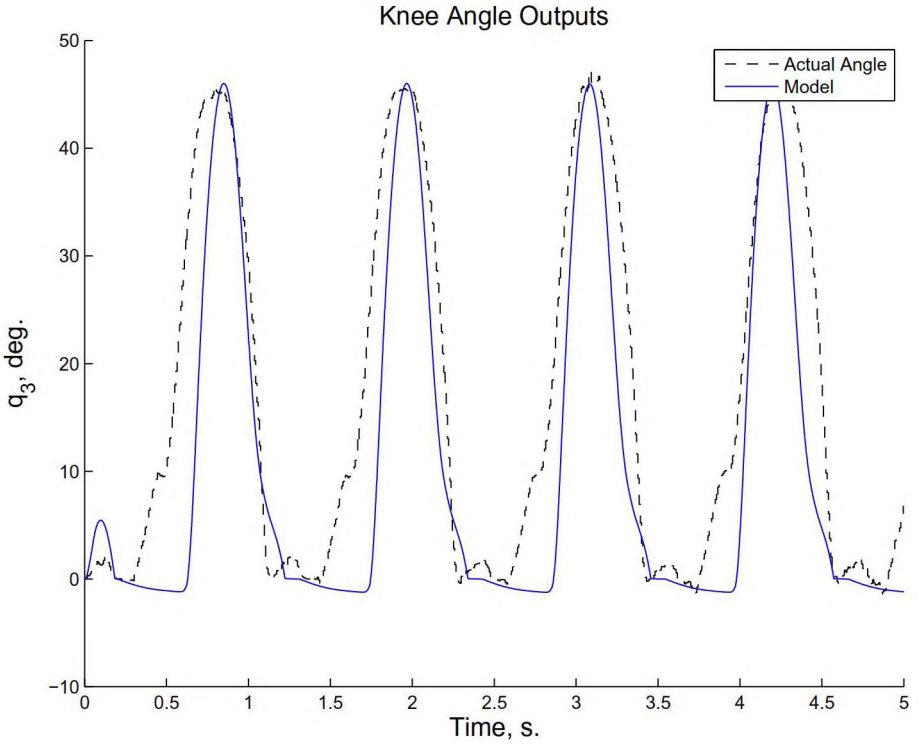

Fig. 8. Comparison between model and experimental outputs: knee angle.

effects such as friction torque. Unmodeled dynamics include gravity torque and inertial coupling. An example of a parametric uncertainty is a value of J subject to uncertainty ΔJ. The uncertainty term can capture this error as $-(\Delta J)\ddot{\theta}$. SMC laws employ the concept of a performance surface, commonly referred to as *sliding manifold*. The sliding manifold is a function s chosen so that desirable tracking performance and reduced or no sensitivity to uncertainties is obtained when the system state is forced to remain in the set $s = 0$. In terms of the tracking error $e = \theta^d - \theta$, the system of Eq. (22) admits a sliding function of the form $s = \dot{e} + \lambda e$, with $\lambda > 0$ a tunable constant. Note that if $s(t) = 0$ for all t after some reaching time t_r, ideal first-order decay is achieved for the tracking error. A frequently-used SMC law capable of achieving and maintaining $s = 0$ in finite time despite the presence of the uncertain term τ_d has the form:

$$u = \frac{J}{k}\left[(\ddot{\theta}^d + \lambda\dot{\theta}^d) + (\frac{b}{J} - \lambda)\dot{\theta} + \eta\,\mathrm{sign}(s)\right], \tag{23}$$

where $\eta > 0$ is chosen according to an assumed bound for τ_d. Note that the motion profiles to be tracked enter the control law through the feedforward term $\ddot{\theta}^d + \lambda\dot{\theta}^d$. Motion profiles used for prosthetic testing are available as data sets, which may be readily differentiated offline to generate the required feedforward term. Implementation of this control law is simpler than that of a PID controller, since no online integration or differentiation are needed, and only position and velocity measurements are required, which are available from optical encoders.

The control law of Eq. (23) was developed using simplified actuator models. Its applicability in actual robot and prosthesis test conditions must be evaluated by simulation studies. Such controller validation was conducted by simulating the controller against the overall model of Section 3.4. Simulation results indicated that the controller would perform well, and that actuator limits would not be surpassed when tracking the planned motion profiles.

6. Real-time control tests

Tests were conducted under pure motion feedback control, using the independent SMCs of Section 5. The robot is initially operated without ground contact, to verify the ability of the control system to track motion profiles without force disturbances. Then, manual bias control on the vertical stage was used to gradually "land" the foot on the treadmill, monitoring the force sensed by the load cell. This was done to evaluate the ability of the control system to operate in the presence of large force disturbances. The speed of the treadmill was manually synchronized to the horizontal velocity of the foot during contact, preventing slippage. Figs. 9 and 10, show the hip displacement and hip swing tracking performance achieved by the

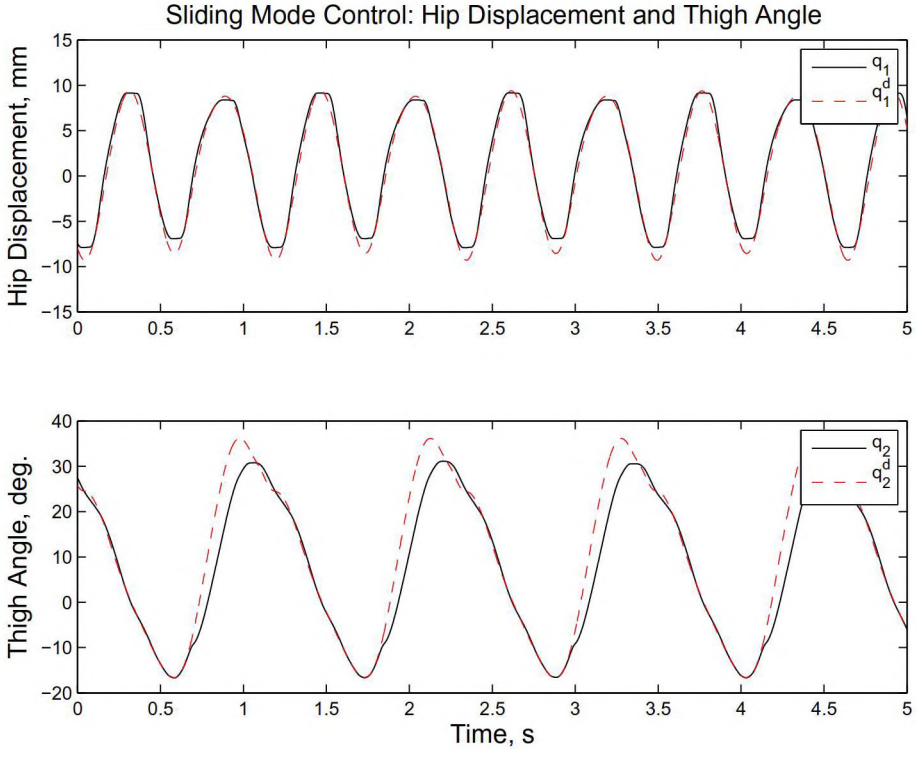

Fig. 9. Hip displacement and thigh angle tracking performance (with ground contact).

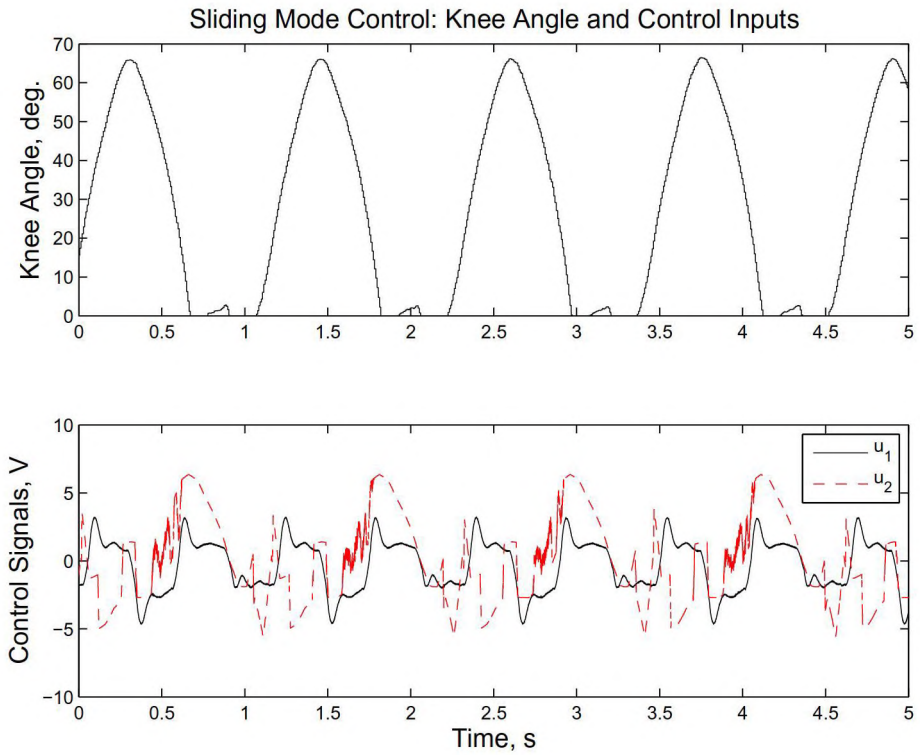

Fig. 10. Knee angle and control voltage histories (with ground contact).

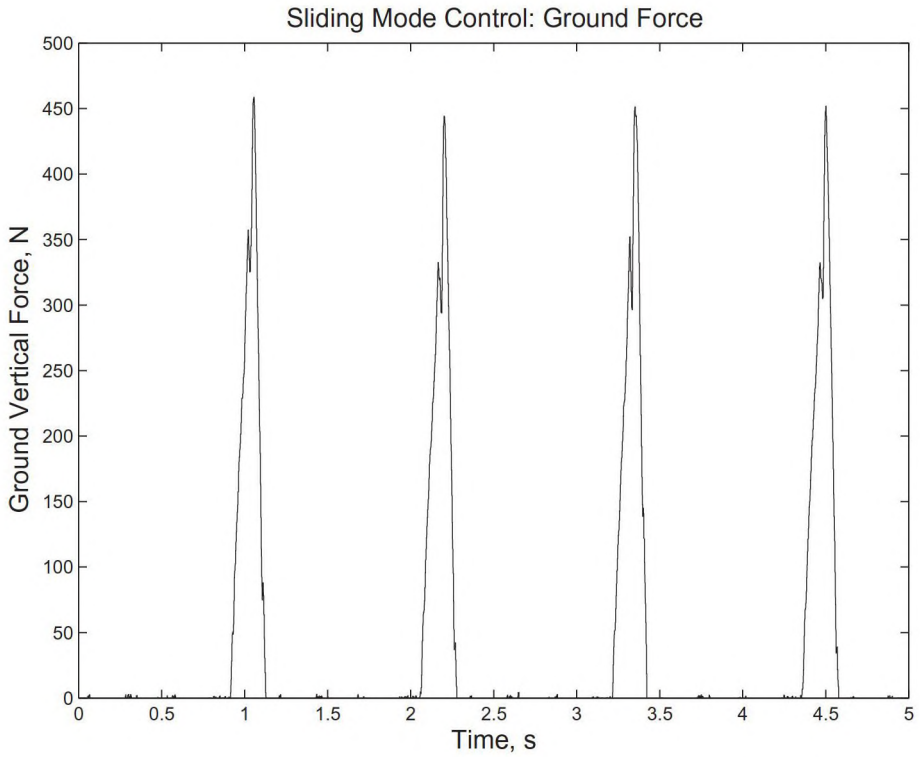

Fig. 11. Vertical ground force.

independent-joint SMC, as well as the measured knee angle and control voltage histories. In this test, manual biasing was applied until a force peak of 450 N was observed. Fig. 11 shows the ground force as measured by the load cell. As expected, the ground forces are only partially compensated by the controller, causing tracking errors for vertical hip displacement and thigh angle during ground contact. Although knee angle is not being controlled, the prosthesis damping mechanism maintains it between 0 and 65 degrees, a range compatible with normal human walking. Note also that the control voltages are within the servo amplifier limits of ± 8 V for the vertical stage and ± 10 V for the rotary stage. The force history shows a double peak, where the higher peak corresponds to flexion of the forefoot. With initial foot contact, ground forces are distributed over a relatively large area, only partly occupied by the load cell. As the foot flexes, the load cell is exposed to most of the distributed force, thus producing a higher reading. Although normal human gait also features a double-peak force profile, our tests have shown that the location of the peaks and their relative magnitudes will be largely influenced by load cell mounting and the phase of gait at the time of ground contact. If force feedback is to be implemented as part of a test, it would be convenient to install a force sensor on the ankle link, converting ground force requirements to ankle force demands.

7. Conclusions

Robot dynamic modeling was successfully used to model both machine and prosthesis, leading to a simulation model than can be used to test control concepts prior to real-time deployment. Other leg prostheses, including with articulated and powered knees and ankles can be interfaced to the machine and their corresponding models integrated. The robot will also prove useful in making objective comparison studies among competing prosthetic designs, since test conditions can be made accurately uniform.

Hazards testing can be conducted to some degree with this design, or with simple modifications. For instance, a treadmill with variable inclination can be used to simulate walking on sloping terrain. The mounting screws on the treadmill may also be adjusted to simulate a banked surface. Steps and surface irregularities can be simulated by replacing the treadmill with a reciprocating horizontal slide, on whose carriage a step can be mounted.

A higher level of realism in robotic testing of transfemoral prostheses may be achieved by adding rotational degrees of freedom to the mechanism. Rotations in the coronal and transverse planes are very small in comparison to hip swing ranges. A spherical mount may be inserted between the vertical carriage and the rotary actuator of this design to enable the additional degrees of freedom. This simple modification would allow testing at various fixed values of the two additional angles. Dynamic changes are likely to require a major re-design, since co-located actuation of several degrees of freedom is problematic. A hexapod platform driven by piezoelectric actuators could be used, if one existed with the required load capacities.

This paper considers pure motion tracking for the hip, and therefore, no claim is made regarding the realism of the sensed force profiles in relation to those arising during normal gait. Force feedback has been used with this robot, however, to reproduce the ground reaction patterns of able-bodied gait [12] even with a passive knee prosthesis. Another relevant control modality is to use impedance control techniques to impose purely a inertial characteristic in vertical axis rather than a pre-determined motion reference. A hip angle motion reference would continue to be tracked in all phases of gait. Vertical impedance control can only be used during the support phase, since there is only one leg. The system would revert to vertical motion tracking when the leg is not in contact with the ground. Under these conditions, ground reaction and hip displacement profiles during the support phase become experimental outcomes that can be used to evaluate a specific prosthetic design.

Acknowledgement

Work supported by the Cleveland Clinic Foundation through the Ohio Third Frontier Program.

Appendix A. Kinematic and dynamic parameters

Velocity Jacobian at load cell location:

$$
\begin{aligned}
&J_e(1,1) = 0,\\
&J_e(1,2) = -(c_3 + l_{cx})\sin(q_2+q_3) + l_{cy}\cos(q_2+q_3) - l_2\sin(q_2),\\
&J_e(1,3) = -(c_3 + l_{cx})\sin(q_2+q_3) + l_{cy}\cos(q_2+q_3),\\
&J_e(2,1) = J_e(2,2) = J_e(2,3) = 0,\\
&J_e(3,1) = 1,\\
&J_e(3,2) = (c_3 + l_{cx})\cos(q_2+q_3) + l_{cy}\sin(q_2+q_3) + l_2\cos(q_2),\\
&J_e(3,3) = (c_3 + l_{cx})\cos(q_2+q_3) + l_{cy}\sin(q_2+q_3).
\end{aligned}
$$

Inertia matrix:

$$
\begin{aligned}
D(1,1) &= m_1 + m_2 + m_3,\\
D(1,2) &= D(2,1) = (c_3\cos(q_2+q_3) + l_2\cos(q_2)) + m_2(c_2\cos(q_2) + l_2\cos(q_2)),\\
D(1,3) &= D(3,1) = c_3 m_3\cos(q_2+q_3),\\
D(2,2) &= I_{2z} + I_{3z} + c_2^2 m_2 + c_3^2 m_3 + l_2^2(m_2+m_3) + 2c_2 l_2 m_2 + 2c_3 l_2 m_3\cos(q_3),\\
D(2,3) &= D(3,2) = m_3 c_3^2 + l_2 m_3\cos(q_3)c_3 + I_{3z},\\
D(3,3) &= m_3 c_3^2 + I_{3z}.
\end{aligned}
$$

c_2 is the distance between the hip rotation axis and the center of mass of link 2. c_3 is the distance between the knee joint and the center of mass of link 3. I_{iz} for $i = 2,3$ is the moment of inertia of link i at its center of mass.

Coriolis/centripetal matrix:

$$
\begin{aligned}
C(1,1) &= 0,\\
C(1,2) &= -\dot{q}_2(l_2 m_3 + m_2(c_2+l_2))\sin(q_2) - c_3 m_3(\dot{q}_2+\dot{q}_3)\sin(q_2+q_3),\\
C(1,3) &= -c_3 m_3\sin(q_2+q_3)(\dot{q}_2+\dot{q}_3),\\
C(2,1) &= 0,\\
C(2,2) &= -c_3 l_2 m_3\dot{q}_3\sin(q_3),\\
C(2,3) &= -c_3 l_2 m_3\sin(q_3)(\dot{q}_2+\dot{q}_3),\\
C(3,1) &= 0,\\
C(3,2) &= c_3 l_2 m_3\dot{q}_2\sin(q_3),\\
C(3,3) &= 0.
\end{aligned}
$$

Gravity vector:

$$
g = \begin{bmatrix} -g(m_1+m_2+m_3) \\ -c_3 g m_3\cos(q_2+q_3) - g(m_2(c_2+l_2)+l_2 m_3)\cos(q_2) \\ -c_3 g m_3\cos(q_2+q_3) \end{bmatrix}. \tag{A.1}
$$

References

[1] Berkeley Robotics and Human Engineering Laboratory. Berkeley Lower Extremity Exoskeleton (BLEEX). <http://bleex.me.berkeley.edu/research/powered-prosthetic-knee/>. Accessed November 2013

[2] J. Laferrier, R. Gailey, Advances in lower-limb prosthetic technology, J. Phys. Med. Rehabil. Clin. North Am. 21 (1) (2010) 87–110.

[3] B. Lawson, H. Varol, M. Goldfarb, Standing stability enhancement with an intelligent powered transfemoral prosthesis, IEEE Trans. Biomed. Eng. 58 (9) (2011) 2617–2624.

[4] E. Martinez-Villalpando, H. Herr, Agonist-antagonist active knee prosthesis: a preliminary study in level-ground walking, J. Rehabil. Res. Dev. 46 (3) (2009) 361–373.

[5] J. Michael, Modern prosthetic knee mechanisms, Clin. Orthop. Relat. Res. 361 (47) (1999) 39–47.

[6] F. Sup, et al., Design and control of an active electrical knee and ankle prosthesis, in: Proc. IEEE. RAS EMBS Int. Conf. Biomed. Robot. Biomechatron., 2008, pp. 523–528.

[7] R. Unal, et al., Towards a fully passive transfemoral prosthesis for normal walking, in: Proc. IEEE. RAS EMBS Int. Conf. Biomed. Robot. Biomechatron., 2012, pp. 1949–1954.

[8] G. Thomas, Evolutionary optimization of artificial neural networks for prosthetic knee control, in: B. Igelnik, J. Zurada (Eds.), Efficiency and Scalability Methods for Computational Intellect, IGI Global, 2013, pp. 142–161.

[9] Fraunhofer Institute for Manufacturing Engineering and Automation, Stuttgart. Orthopaedics and motion systems. <http://ipa.fraunhofer.de/OrthopaedicsandMotionSystems.83.0.html?&L=2>. Accessed November 2013.

[10] Cleveland Clinic Lerner Research Institute. Neuromusculoskeletal simulator. <http://mds.clevelandclinic.org/Services/BioRobotics/Services.aspx>. Accessed November 2013

[11] Richter, H., 2013. Development of a leg prosthesis test robot, lab report. <http://academic.csuohio.edu/richterh/lab/ccfrobot/>. Accessed June 2014.

[12] R. Davis, H. Richter, D. Simon, A. van den Bogert, Evolutionary ground reaction force optimization of a prosthetic leg testing robot, in: Proc. 2014 American Control Conference, 2014, Portland.

[13] M. Bellmann, T. Schmalz, S. Blumentritt, Comparative biomechanical analysis of current microprocessor-controlled prosthetic knee joints, Arch. Phys. Med. Rehabil. 91 (4) (2010) 644–652.

[14] T. Chin et al, Comparison of different microprocessor controlled knee joints on the energy consumption during walking in trans-femoral amputees: intelligent knee prosthesis (ip) versus c-leg, Prosthet. Orthot. Int. 30 (1) (2006) 73–80.

[15] J. Johansson et al, A clinical comparison of variable-damping and mechanically passive prosthetic knee devices, Am. J. Phys. Med. Rehabil. 84 (8) (2005) 563–575.

[16] A. Segal et al, Kinematic and kinetic comparisons of transfemoral amputee gait using C-Leg and Mauch SNS prosthetic knees, J. Rehabil. Res. Dev. 43 (7) (2006) 857–870.

[17] R.E. Seroussi et al, "Mechanical work adaptations of above-knee amputee ambulation", Arch. Phys. Med. Rehabil. 77 (11) (1996) 1209–1214.

[18] A. van den Bogert, S. Samorezov, B. Davis, W. Smith, Modeling and optimal control of an energy-storing prosthetic knee, ASME J. Biomech. Eng. 134 (5) (2012) 051007.

[19] M. Spong, S. Hutchinson, M. Vidyasagar, Robot Modeling and Control, Wiley, 2006.

[20] J. Denavit, R. Hartenberg, A kinematic notation for lower-pair mechanisms based on matrices, Trans. ASME J. Appl. Mech. 23 (1955) 215–221.

[21] J. Shigley, C. Mischke, Mechanical Design Engineering, McGraw-Hill, 1989.

[22] E. Knox, The Role of Prosthetic Feet in Walking (Ph.D. thesis), Northwestern University, 1996.

[23] P. Mahmoodi, R. Ransing, M. Friswell, Modelling the effect of heel to toe roll-over contact on the walking dynamics of passive biped robots, Appl. Math. Model. 37 (2013) 7352–7373.
[24] S. Srinivasan, E. Westervelt, H. Hansen, A low-dimensional sagittal-plane forward-dynamic model for asymmetric gait and its application to study the gait of transtibial prosthesis users, ASME J. Biomech. Eng. 131 (3) (2009).
[25] A. Slocum, Precision Machine Design, Society of Manufacturing, 1992.
[26] C. Edwards, S. Spurgeon, Sliding Mode Control: Theory and Applications, Taylor and Francis, 1998.
[27] J. Slotine, W. Li, Applied Nonlinear Control, Prentice Hall, 1990.
[28] V. Utkin, Sliding Modes in Control Optimization, Springer-Verlag, 1992.

Post-print standardized by MSL Academic Endeavors, the imprint of the Michael Schwarts Library at Cleveland State University, 2018